

Editorial Manager(tm) for Nanoscale Research Letters
Manuscript Draft

Manuscript Number:

Title: Thermal induced nano-structural and optical changes of nc-Si:H deposited by hot-wire CVD

Article Type: Original Research - Nano Express

Keywords: Hot-wire CVD; quantum size effects; nano-crystallite; optical band gap

Corresponding Author: Dr Christopher Joseph Arendse, PhD

Corresponding Author's Institution: CSIR National Centre for Nano-Structured Materials, P. O. Box 395, Pretoria 0001, South Africa

First Author: Christopher Joseph Arendse, PhD

Order of Authors: Christopher Joseph Arendse, PhD; Gerald F Malgas, PhD; Theo F Muller, MSc; Dirk Knoesen, PhD; Clive J Oliphant, MSc; Clive J Oliphant, MSc; David E Motaung, MSc; David E Motaung, MSc; Gerald F Malgas, PhD; Bonex W Mwakikunga, MSc; Bonex W Mwakikunga, MSc; Bonex W Mwakikunga, MSc

1
2
3
4 **Thermal induced nano-structural and optical changes of nc-Si:H**
5
6 **deposited by hot-wire CVD**
7
8
9

10 C. J. Arendse^{1,*}, G. F. Malgas¹, T. F. G. Muller², D. Knoesen², C. J.
11
12 Olpivant^{1,2}, D. E. Motaung^{1,2} and B. W. Mwakikunga^{1,3,4}
13
14
15

16
17
18 ¹CSIR National Centre for Nano-Structured Materials, P. O. Box 395, Pretoria
19
20 0001, South Africa
21

22 ²Department of Physics, University of the Western Cape, Private Bag X17,
23
24 Bellville 7535, South Africa
25

26
27 ³School of Physics, University of the Witwatersrand, Private Bag 3, P. O.
28
29 Wits, Johannesburg 2050, South Africa
30

31 ⁴Department of Physics, University of Malawi, The Polytechnic, Private Bag
32
33 303, Blantyre, Malawi
34
35
36
37

38 **Abstract**
39

40 We report on the thermal induced changes of the nano-structural and optical
41
42 properties of hydrogenated nanocrystalline silicon in the temperature range
43
44 200 – 700 °C. The as-deposited sample has a high crystalline volume fraction
45
46 of 53% with an average crystallite size of ~ 3.9 nm, where 66% of the total
47
48 hydrogen is bonded as ≡Si–H monohydrides on the nano-crystallite surface. A
49
50 growth in the native crystallite size and crystalline volume fraction occurs at
51
52 annealing temperatures ≥ 400 °C, where hydrogen is initially removed from
53
54 the crystallite grain boundaries followed by its removal from the amorphous
55
56
57
58

59
60

^{*} Corresponding author: C. J. Arendse (CArendse@csir.co.za)
61 Tel: +27 12 841 3671, Fax: +27 12 841 2229
62
63
64
65

1
2
3
4 network. The nucleation of smaller nano-crystallites at higher temperatures
5
6 accounts for the enhanced porous structure and the increase in the optical
7
8 band gap and average gap.
9

10 11 12 **Keywords**

13
14
15 Hot-wire CVD, quantum size effects, nano-crystallite, optical band gap
16
17

18 19 20 **1. Introduction**

21
22
23
24 Hydrogenated nanocrystalline silicon (nc-Si:H) has been the subject of
25
26 intense scientific and technological interest over the past decade, mainly due
27
28 to its reduced photo-induced degradation [1], efficient visible
29
30 photoluminescence [2], tailored optical band gap [3], increased conductivity
31
32 and greater doping efficiency [4]. It has been highlighted that these unique
33
34 features are a direct cause of the quantum size effects of the silicon nano-
35
36 crystallites. These improvements make nc-Si:H a potential candidate for
37
38 application in photovoltaic and opto-electronic devices [5, 6].
39
40
41
42
43

44
45 The hot-wire chemical vapour deposition (HWCVD) technique, based on the
46
47 catalytic decomposition of the precursor gasses by a heated transition metal
48
49 filament, has been established as a viable deposition technique for nc-Si:H
50
51 thin films [6-7]. The structural and opto-electronic properties of the thin films
52
53 are dependent on the deposition parameters, of which the hydrogen dilution
54
55 and substrate temperature are the most crucial. It has been established that
56
57 the etching effect of atomic hydrogen, created by the catalytic decomposition
58
59
60
61
62
63
64
65

1
2
3
4 of H₂, is responsible for the termination of weak Si–Si bonds from the surface
5
6 and sub-surface regions and that the nucleation of the nano-crystallites are
7
8 improved by increasing the hydrogen dilution [7-10]. It has also been reported
9
10 that the hydrogen dilution during deposition determines the concentration and
11
12 the distribution of hydrogen in nc-Si:H, which is closely related to the nano-
13
14 structural features; i.e. crystallite size and crystalline volume fraction [11-14].
15
16 These nano-structural features eventually determine the optical properties of
17
18 the material. In particular, the quantum size effects of the Si nano-crystallites
19
20 and the hydrogen concentration have a strong correlation with the optical
21
22 band gap [15-16].
23
24
25
26
27
28

29 An investigation into the role of hydrogen in nc-Si:H is therefore crucial for
30
31 the understanding of its relation to the nano-structure and the optical
32
33 properties. In this contribution, we investigate the effects of the hydrogen
34
35 concentration and bonding configuration in nc-Si:H deposited by HWCVD on
36
37 the nano-structural features and the optical properties. The hydrogen
38
39 concentration and bonding configuration were controlled by post-deposition
40
41 isochronal annealing.
42
43
44
45
46

47 **2. Experimental**

48
49
50
51

52 The nc-Si:H thin film was deposited by the HWCVD process simultaneously
53
54 on single-side polished <100> crystalline silicon and Corning 7059 substrates,
55
56 using a mixture of 4 sccm SiH₄ and 26 sccm H₂ decomposed by seven
57
58 parallel tungsten filaments, 15 cm apart and 36 cm away from the substrates.
59
60
61
62
63
64
65

1
2
3
4 A detailed description of the experimental set-up is given elsewhere [17-18].
5
6 The filament temperature, substrate temperature and deposition pressure
7
8 were fixed at 1600 °C, 420 °C and 60 μbar, respectively. The as-deposited
9
10 nc-Si:H thin film was ~ 1140 nm-thick, as measured using a Veeco®
11
12 profilometer.
13
14

15
16
17
18 Subsequent annealing was performed under high-purity, flowing N₂ gas in a
19
20 tube furnace at annealing temperatures (T_A) ranging from 200 – 700 °C in 100
21
22 °C increments. The N₂ flow rate, heating rate and dwell time for all
23
24 temperatures amounted to 300 sccm, 10°C/min and 30 minutes, respectively.
25
26 After each annealing temperature, the thin film was allowed to cool to room
27
28 temperature in the tube furnace, while maintaining the N₂ flow rate. Thereafter
29
30 the required analytical techniques were performed.
31
32

33
34
35
36 Fourier transform infrared (FTIR) absorption spectra were collected in
37
38 transmission geometry from 400 – 4000 cm⁻¹ with a spectral resolution of 1
39
40 cm⁻¹, using a Perkin-Elmer Spectrum 100 FTIR spectrophotometer. The
41
42 structural properties were investigated using a Jobin-Yvon HR800 micro-
43
44 Raman spectrometer in backscattering geometry at room temperature. The
45
46 Raman spectra were collected in the region 100 – 1000 cm⁻¹ with a spectral
47
48 resolution of 0.4 cm⁻¹, using an excitation wavelength of 514.5 nm. X-ray
49
50 diffraction (XRD) spectra were collected in reflection geometry at 2θ-values
51
52 ranging from 10 – 90° with a step size of 0.02°, using a Phillips PW 1830 x-ray
53
54 powder diffractometer operating at 45 kV and 40 mA. Copper K_{α1} radiation
55
56 with a wavelength of 1.5406 Å was used as the x-ray source. Optical
57
58
59
60
61
62
63
64
65

1
2
3
4 transmission spectra were measured from 200 – 900 nm with a spectral
5
6 resolution of 1nm, using a Perkin-Elmer LS75S UV/VIS spectrophotometer.
7
8
9

10 **3. Results and Discussion**

11 **3.1 Nano-structural properties**

12
13
14
15 FTIR spectroscopy is the established analytical technique of choice to
16
17 probe the silicon-hydrogen bonding configurations and to calculate the
18
19 hydrogen concentration in nc-Si:H and related material. The FTIR absorption
20
21 spectrum of the sample in the as-deposited state is shown in Fig. 1. The
22
23 strong absorption bands in the region 920 – 1250 cm^{-1} is associated with the
24
25 asymmetric Si–O–Si stretching vibration [19], whereas the peak centred
26
27 around 2250 cm^{-1} is assigned to the H–SiO₃ vibration [20]. This is indicative
28
29 of an oxidation effect caused by its porous-like microstructure, which is a
30
31 typical feature for nc-Si:H thin films [21-22]. The enhanced absorption band
32
33 centred around 640 cm^{-1} is attributed to the rocking vibrations of all bonding
34
35 configurations of Si–H_x [23]. The absorption bands in the region 1900 – 2150
36
37 cm^{-1} is a result of the convolution of several absorption bands associated with
38
39 the stretching vibrations of Si–H_x in different configurations. This is illustrated
40
41 in the insert of Fig. 1, where the absorption spectrum is decomposed into
42
43 three Gaussian components. The absorption peaks centred around 1985 cm^{-1}
44
45 and 2090 cm^{-1} are assigned to the stretching vibrations of ≡Si–H
46
47 monohydrides in the amorphous network (isolated) and on the surface of the
48
49 Si nano-crystallites (clustered), respectively [21, 24]. The weak absorption
50
51
52
53
54
55
56
57
58
59
60
61
62
63
64
65

1
2
3
4 band centred at $\sim 2130 \text{ cm}^{-1}$ is assigned to the existence of $(=\text{Si}=\text{H}_2)_n$
5
6 polyhydride complexes on Si nano-crystallite grain boundaries [25-26].
7
8
9

10
11 To quantify the fraction of H bonded on the surface of nano-crystallites in
12 nc-Si:H, we define a structure factor, $R_s = I_{2090} / [I_{1985} + I_{2090} + I_{2130}]$, where I
13 denotes that integrated intensity of each decomposed peak. The total bonded
14 hydrogen concentration (C_H) was estimated from the integrated absorption of
15 the 640 cm^{-1} rocking mode using previous reported procedures [27-28]. In the
16 as-deposited state, C_H amounts to $\sim 2 \text{ at.}\%$, characteristic for nc-Si:H
17 deposited with high hydrogen dilution [16, 29], where $\sim 66\%$ thereof is bonded
18 on the surface of the nano-crystallites. We propose that this relatively high
19 value for R_s is indicative of a high crystalline volume fraction.
20
21
22
23
24
25
26
27
28
29
30
31

32
33
34 Fig. 2 shows the plots of the hydrogen concentration and the structure factor
35 as a function of annealing temperature. The hydrogen concentration and
36 structure factor are relatively constant at temperatures below $400 \text{ }^\circ\text{C}$,
37 demonstrating that the nano-structure is stable in this temperature regime.
38 After annealing at $400 \text{ }^\circ\text{C}$ most of the $(=\text{Si}=\text{H}_2)_n$ polyhydride bonds on the
39 grain boundaries of the Si nano-crystallites have been terminated and
40 consequently results in an increase in the structure factor. Annealing at higher
41 temperatures induce a significant decrease in C_H , coupled with an increase in
42 R_s . These changes are caused by the preferential termination of the isolated
43 $\equiv\text{Si}-\text{H}$ bonds in the amorphous network. We propose that the instability
44 induced at $T_A \geq 400 \text{ }^\circ\text{C}$ is related to the growth of the native nano-crystallites
45 and to the nucleation of nano-crystallites in the amorphous network, thereby
46
47
48
49
50
51
52
53
54
55
56
57
58
59
60
61
62
63
64
65

1
2
3
4 resulting in an increase in the crystalline volume fraction. It should be noted
5
6 that no Si-H_x absorption peaks were identified after annealing at 700 °C.
7
8
9

10
11 Raman spectroscopy provides direct nano-structural information
12
13 quantitatively related to the average nano-crystallite size and the crystalline
14
15 volume fraction in nc-Si:H. Fig. 3 shows the Raman spectra of the sample in
16
17 the as-deposited state and after annealing at specific temperatures. All
18
19 spectra display the following main features: (i) a sharp peak centred around
20
21 515 cm⁻¹, associated with the transverse optic (TO) mode of the nc-Si phase;
22
23 (ii) the broad shoulder centred around 480 cm⁻¹, due to the TO-mode of the
24
25 amorphous silicon (a-Si) phase; and (iii) a smaller shoulder around 505 cm⁻¹,
26
27 corresponding to the distribution of crystalline grain boundaries in the sample.
28
29
30
31
32

33
34 The crystalline volume fraction, $f_c = [A_{505} + A_{515}] / [A_{480} + A_{505} + A_{515}]$, can be
35
36 estimated from the integrated areas of the afore-mentioned deconvoluted
37
38 Gaussian peaks [30]. The crystallite size is empirically calculated from
39
40 $d_{\text{Raman}} = 2\pi\sqrt{B/\Delta\omega}$, where $\Delta\omega$ is the shift of the 515 cm⁻¹ peak relative to the
41
42 c-Si peak at 520 cm⁻¹ and $B = 2.0 \text{ cm}^2$ [31]. The quantitative Raman results
43
44 are summarized in Table 1. In the as-deposited state, the average crystallite
45
46 size and the crystalline volume fraction amounts to about 3.9 nm and 53%,
47
48 respectively, and remain relatively constant after annealing at 300 °C. These
49
50 observations reiterate that the nano-structure of the sample remains stable at
51
52 temperatures below 400 °C. A blue shift of the nc-Si TO-peak, accompanied
53
54 with a reduction in the intensity of the a-Si TO-peak is observed at annealing
55
56 temperatures ≥ 400 °C, indicative of an increase in the crystallite size and the
57
58
59
60
61
62
63
64
65

1
2
3
4 crystalline volume fraction, respectively, and supports the claims based on the
5
6 FTIR results.
7
8
9

10 XRD was employed as a complimentary method to qualitatively probe the
11 changes in the crystallinity as a function of annealing temperature (see Fig.
12 4). Three preferential orientations in the $\langle 111 \rangle$, $\langle 200 \rangle$ and $\langle 311 \rangle$ directions
13 are observed. The crystallite size in the as-deposited state, estimated from
14 the full-width-half-maximum (FWHM) of the (111)-peak, amounts to ~ 19.5 nm
15 [32]. A narrowing in the FWHM of the (111)-peak, accompanied with an
16 increase in its intensity is observed with an increase in annealing temperature.
17 This confirms the increase of the crystallite size and crystalline volume
18 fraction, as probed by Raman spectroscopy.
19
20
21
22
23
24
25
26
27
28
29
30
31
32
33

34 The thermal induced nano-structural changes of the nc-Si:H thin film can be
35 interpreted as follows, based on the variation of the Si-H_x bonding and the
36 crystalline character. In the as-deposited state the crystalline volume fraction
37 is relatively large and therefore the majority of H is bonded to the surface of
38 the nano-crystallites. The nano-structural properties are stable at
39 temperatures below 400 °C, attributed to its large crystalline volume fraction.
40 An initial increase in the native crystallite size is observed after annealing at
41 400 °C, resulting in the removal of hydrogen from the grain boundaries. It is
42 also feasible that smaller crystallites have coalesced into larger crystallites. At
43 higher temperatures, hydrogen is removed preferentially from the amorphous
44 phase, indicative of the nucleation of smaller nano-crystallites of size < 3 nm
45 in the amorphous network [33], undetected by Raman spectroscopy and XRD.
46
47
48
49
50
51
52
53
54
55
56
57
58
59
60
61
62
63
64
65

3.2 Optical properties

The optical properties were determined from UV-visible transmission measurements, using the method proposed by Swanepoel [34-35]. The thickness of the as-deposited sample was calculated to be ~ 1180 nm, which concurs to that measured by profilometry. The refractive index $n(\nu)$ of a material is an important optical parameter, since it is directly proportional to density [36]. Fig. 5 shows the spectral dependence of the calculated refractive index for the sample in the as-deposited state and after annealing at specific temperatures. A slight increase in the refractive index is observed after annealing at 400 °C, followed by a decrease at higher temperatures. The initial increase can be ascribed to the increase in the native crystallite size and possibly due to the coalescence of smaller nano-crystallites. Furthermore, the presence of $(=Si=H_2)_n$ complexes in the as-deposited state is indicative of a disordered, porous material and the removal thereof after 400 °C would therefore result in a more compact material. The subsequent decrease of the refractive index at higher temperatures is attributed to a more porous structure, possibly caused by the nucleation of smaller nano-crystallites in the amorphous network. Similar trends in the refractive index at zero photon energy (n_0) are observed (see Table 1).

Detailed analysis of the refractive index spectra were performed using the suggested model of Wemple et al [37]. At energies below than of the optical band gap, the refractive index is related to the square of the photon energy $(h\nu)^2$ by:

$$n^2(\nu) = 1 + \frac{E_M E_D}{E_M^2 - (h\nu)^2} \quad (1)$$

where E_M and E_D is the average gap and dispersion energy, respectively. The plot of $1/[n^2(\nu)-1]$ versus $(h\nu)^2$ allows for the determination of E_M , E_D and n_0 . The extrapolated results of n_0 and E_M , calculated from the linear fit through the data, are listed in Table 1.

The spectral dependence of the absorption coefficient $\alpha(\nu)$ for the sample in the as-deposited state and after annealing at specific temperatures is depicted in Fig. 6. The optical band gap, referred to as E_{04} , is defined as the photon energy where $\alpha(\nu) = 10^4 \text{ cm}^{-1}$, and the values thereof are reported in Table 1. A red shift in E_{04} is observed for $T_A \leq 600 \text{ }^\circ\text{C}$ followed by an unexpected blue shift after annealing at $700 \text{ }^\circ\text{C}$. It is established that the optical band gap of hydrogenated amorphous silicon (a-Si:H) deposited by HWCVD and PECVD increases with an increase in the hydrogen concentration [7, 38]. It should be noted that the optical band gap for the sample in the as-deposited state is larger than that of a-Si:H with similar C_H values. This discrepancy is due to the presence of nano-crystallites in the amorphous network, which lowers the absorption in nc-Si:H and shifts the optical band gap towards higher energies [15-16]. The quantum size effect size also predicts that an increase in crystallite size is associated with a decrease in the optical band gap. The initial decrease in E_{04} after $400 \text{ }^\circ\text{C}$ is due to the combined effect of the decreased C_H and the growth in the crystallite size. After annealing at $600 \text{ }^\circ\text{C}$ the initial hydrogen concentration

1
2
3
4 has decreased by ~ 90% with about the same incremental increase in the
5
6 crystallite size as at 400 °C, and therefore a more notable decrease in E_{04} is
7
8 expected. However, a minute 0.03 eV decrease in E_{04} is observed and is
9
10 attributed to the nucleation of smaller nano-crystallites in the amorphous
11
12 network, which explains the competing increasing effect on E_{04} . After
13
14 annealing at 700 °C, where no hydrogen was detected by FTIR spectroscopy,
15
16 this effect is more pronounced in that an increase in the optical band gap is
17
18 observed.
19
20
21
22
23

24
25 The optical band gap and the average gap (E_M) have similar behaviours with
26
27 respect to annealing temperature, thereby implying that the growth of the
28
29 native nano-crystallites and the nucleation of smaller crystallites in the
30
31 amorphous network have similar effects on the band edges and on the
32
33 conduction and valence bands. Therefore, the average gap can be used to
34
35 describe the thermal induced changes in the optical properties of nc-Si:H.
36
37
38
39
40

41 **4. Conclusion**

42
43
44

45 The effect of isochronal annealing on the nano-structural and optical
46
47 properties of nc-Si:H, with the emphasis on its relation to the hydrogen
48
49 distribution and concentration, was investigated. Initial changes in the nano-
50
51 structure are observed after annealing at 400 °C, as evident by termination of
52
53 $(=Si=H_2)_n$ polyhydrides from the grain boundaries caused by the growth of the
54
55 native nano-crystallites. At higher temperatures, a further increase in the
56
57 native nano-crystallite size and the crystalline volume fraction is observed,
58
59
60
61
62
63
64
65

1
2
3
4
5
6
7
8
9
10
11
12
13
14
15
16
17
18
19
20
21
22
23
24
25
26
27
28
29
30
31
32
33
34
35
36
37
38
39
40
41
42
43
44
45
46
47
48
49
50
51
52
53
54
55
56
57
58
59
60
61
62
63
64
65

accompanied with the nucleation of smaller nano-crystallites and the subsequent removal of hydrogen from the amorphous network. At temperatures ≥ 600 °C the nucleation of the smaller nano-crystallites results in a porous material with an increased optical band gap and average gap, explained by the quantum size effect.

Acknowledgements

The authors acknowledge the financial assistance of the Department of Science and Technology, the National Research Foundation and the Council for Scientific and Industrial Research (Project no: HGERA2S) of South Africa.

1
2
3
4 **References**
5
6
7

- 8 [1] V. Shah, J. Meier, E. Vallat-Sauvain, N. Wyrsh, U. Kroll, C. Droz and U.
9 Graf, *Sol. Energy Mater. & Sol. Cells* 78, 469 (2003)
10
11 [2] H. Takagi, H. Ogawa, Y. Yamazabi, A. Ishizaki, T. Nakakiri, *Appl. Phys.*
12 *Lett.* 56, 2379 (1990)
13
14 [3] J. Kitao, H. Harada, N. Yoshida, Y. Kasuya, M. Nishio, T. Sakamoto, T.
15 Itoh, S. Nonomura, *Sol. Energy Mater. & Sol. Cells* 66, 245 (2001)
16
17 [4] R. Saleh, N.H. Nickel, *Thin Solid Films* 427, 266 (2003)
18
19 [5] S. Guha, J. Yang, D.L. Williamson, Y. Lubianiker, J.D. Cohen, A.H.
20 Mahan, *Appl. Phys. Lett.* 74, 1860 (1999)
21
22 [6] R.E.I. Schropp, H. Li, R.H. Franken, J.K. Rath, C.H.M. van der Werf,
23 J.W.A. Schüttauf, R.L. Stolk, *Thin Solid Films* 516, 6818 (2008)
24
25 [7] K.F. Feenstra, R.E.I. Schropp, W.F. van der Weg, *J. Appl. Phys.* 85,
26 6843 (1999)
27
28 [8] P. Brogueira, J.P. Conde, S. Arekat, V. Chu, *J. Appl. Phys.* 79, 8748
29 (1996)
30
31 [9] S. Halindintwali, D. Knoesen, R. Swanepoel, B.A. Julies, C. Arendse, T.
32 Muller, C.C. Theron, A. Gordijn, P.C.P. Bronsveld, J.K. Rath, R.E.I.
33 Schropp, *Thin Solid Films* 515, 8040 (2007)
34
35 [10] S.K. Kim, K.C. Park, J. Jang, *J. Appl. Phys.* 77, 5115 (1995)
36
37 [11] H. Li, R.H. Franken, R.L. Stolk, C.H.M. van der Werf, J.K. Rath, R.E.I.
38 Schropp, *J. Non-Cryst. Solids* 354, 2087 (2008)
39
40 [12] S. Zhang, X. Liao, Y. Xu, R. Martins, E. Fortunato, G. Kong, *J. Non-*
41 *Cryst. Solids* 338–340, 188 (2004)
42
43
44
45
46
47
48
49
50
51
52
53
54
55
56
57
58
59
60
61
62
63
64
65

- 1
2
3
4 [13] J.-H. Shim, Seongil Im, N.-H. Cho, *Appl. Surf. Sci.* 234, 268 (2004)
5
6 [14] R. Amrani, D. Benlekehal, R. Baghdad, D. Senouci, A. Zeinert, K.
7
8 Zellama, L. Chahed, J.D. Sib, Y. Bouizem, *J. Non-Cryst. Solids* 354 ,
9
10 2291 (2008)
11
12 [15] A.M. Ali, S. Hasegawa, *Thin Solid Films* 437, 68 (2003)
13
14 [16] A.M. Funde, N.A. Bakr, D.K. Kamble, R.R. Hawaldar, D.P. Amalnerkar,
15
16 S.R. Jadkar, *Sol. Energy Mater. & Sol. Cells* 92, 1217 (2008)
17
18 [17] C.J. Arendse, D. Knoesen, D.T. Britton, *Thin Solid Films* 501, 92 (2006)
19
20 [18] D. Knoesen, C. Arendse, S. Halindintwali, T. Muller, *Thin Solid Films*
21
22 516, 822 (2008)
23
24 [19] Montero, L. Galan, O. Najmi, and J. M. Albella, *Phys. Rev. B* 50, 4881
25
26 (1994)
27
28 [20] G. Lucovsky, J. Yang, S. S. Chao, J. E. Tyler, and W. Czubaty, *Phys.*
29
30 *Rev. B* 28, 3225 (1983)
31
32 [21] D. Han, K. Wang, J. M. Owens, *J. Appl. Phys.* 93, 3776 (2003)
33
34 [22] S. Halindintwali, D. Knoesen, R. Swanepoel, B.A. Julies, C. Arendse, T.
35
36 Muller, C. C. Theron, A. Gordijn, P. C. P. Bronsveld, J. K. Rath, R. E. I.
37
38 Schropp, *Thin Solid Films* 515, 8040 (2007)
39
40 [23] G. Lucovsky, Z. Zing, Z. Lu, D. R. Lee and J. L. Whitten, *J. Non-Cryst.*
41
42 *Solids* 182, 90 (1995)
43
44 [24] J. K. Rath, H. Meiling and R. E. I. Schropp, *Jpn. J. Appl. Phys.* 36, 5436
45
46 (1997)
47
48 [25] C. Gonaves, S. Charvet, A. Zeinert, M. Clin, K. Zellama, *Thin Solid Films*
49
50 403-404, 91 (2002)
51
52
53
54
55
56
57
58
59
60
61
62
63
64
65

- 1
2
3
4 [26] D. Stryahilev, F. Diehl, B. Schroeder, *J. Non-Cryst. Solids* 266–269, 166
5
6 (2000)
7
8 [27] M. H. Brodsky, M. Cardona, and J. J. Cuomo, *Phys. Rev. B* 16, 3556
9
10 (1977)
11
12 [28] H. Shanks, C. J. Fang, L. Ley, M. Cardona, F. J. Desmond, and S.
13
14 Kalbitzer, *Phys. Status Solidi B* 100, 43 (1980)
15
16 [29] U. Kroll, J. Meier, A. Shah, S. Mikhailov, and J. Waber, *J. Appl. Phys.* 80,
17
18 4971 (1996)
19
20 [30] T. Kaneko, M. Wakagi, K. Onisawa, T. Minemura, *Appl. Phys. Lett.* 64,
21
22 1865 (1994)
23
24 [31] Y. He, C. Yin, G. Cheng, L. Wang, X. Liu, G.Y. Hu, , *J. Appl. Phys.* 75,
25
26 797 (1994)
27
28 [32] H.P. Klung, L.E. Alexander, *X-ray Diffraction Procedures*, Wiley, New
29
30 York, 1974.
31
32 [33] E. Bustarret, M.A. Hachicha, M. Brunel, *Appl. Phys. Lett.* 52, 1675 (1988)
33
34 [34] R. Swanepoel, *J. Phys. E: Sci. Instrum.* 16, 1214 (1983)
35
36 [35] R. Swanepoel, *J. Phys. E: Sci. Instrum.* 17, 896 (1984)
37
38 [36] E.C. Freeman, W. Paul, *Phys. Rev. B* 5, 3017 (1972)
39
40 [37] S.H. Wemple, M. Didomenico, *Phys. Rev. B* 3, 1338 (1971)
41
42 [38] M. Yamaguchi, K. Moigaki, *Phil. Mag. B* 79, 387 (1999)
43
44
45
46
47
48
49
50
51
52
53
54
55
56
57
58
59
60
61
62
63
64
65

Figure 1
[Click here to download high resolution image](#)

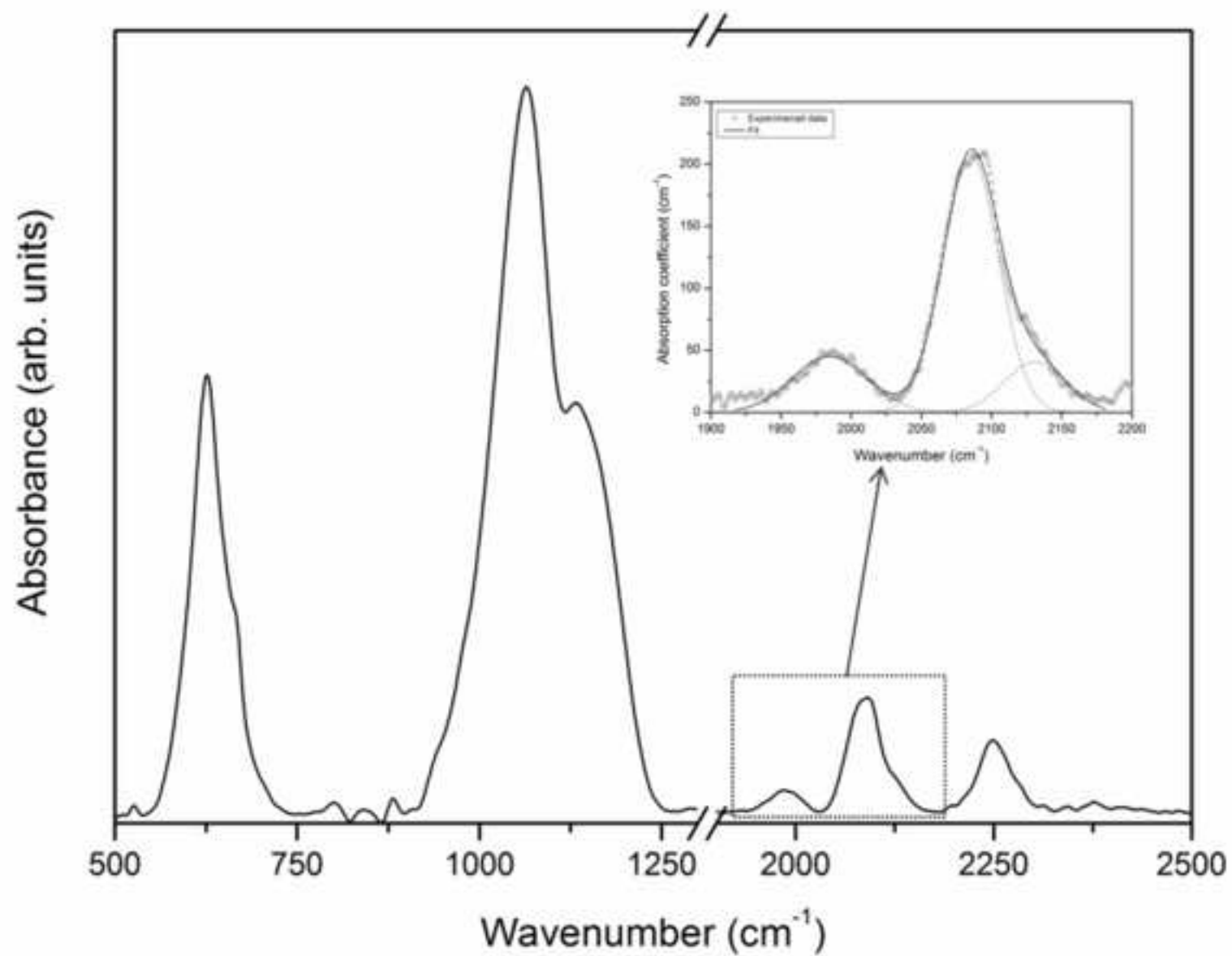


Figure 2
[Click here to download high resolution image](#)

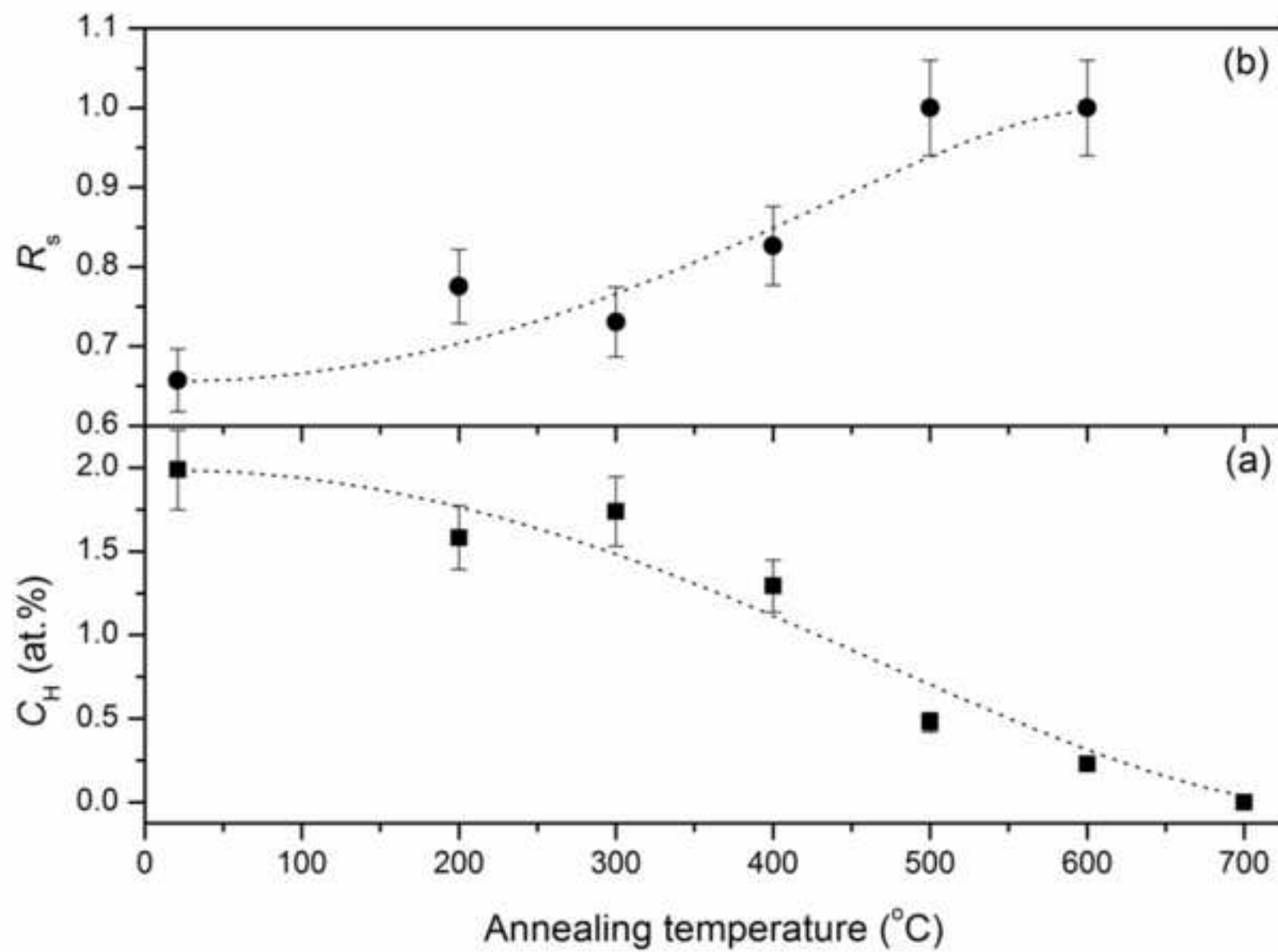


Figure 3
[Click here to download high resolution image](#)

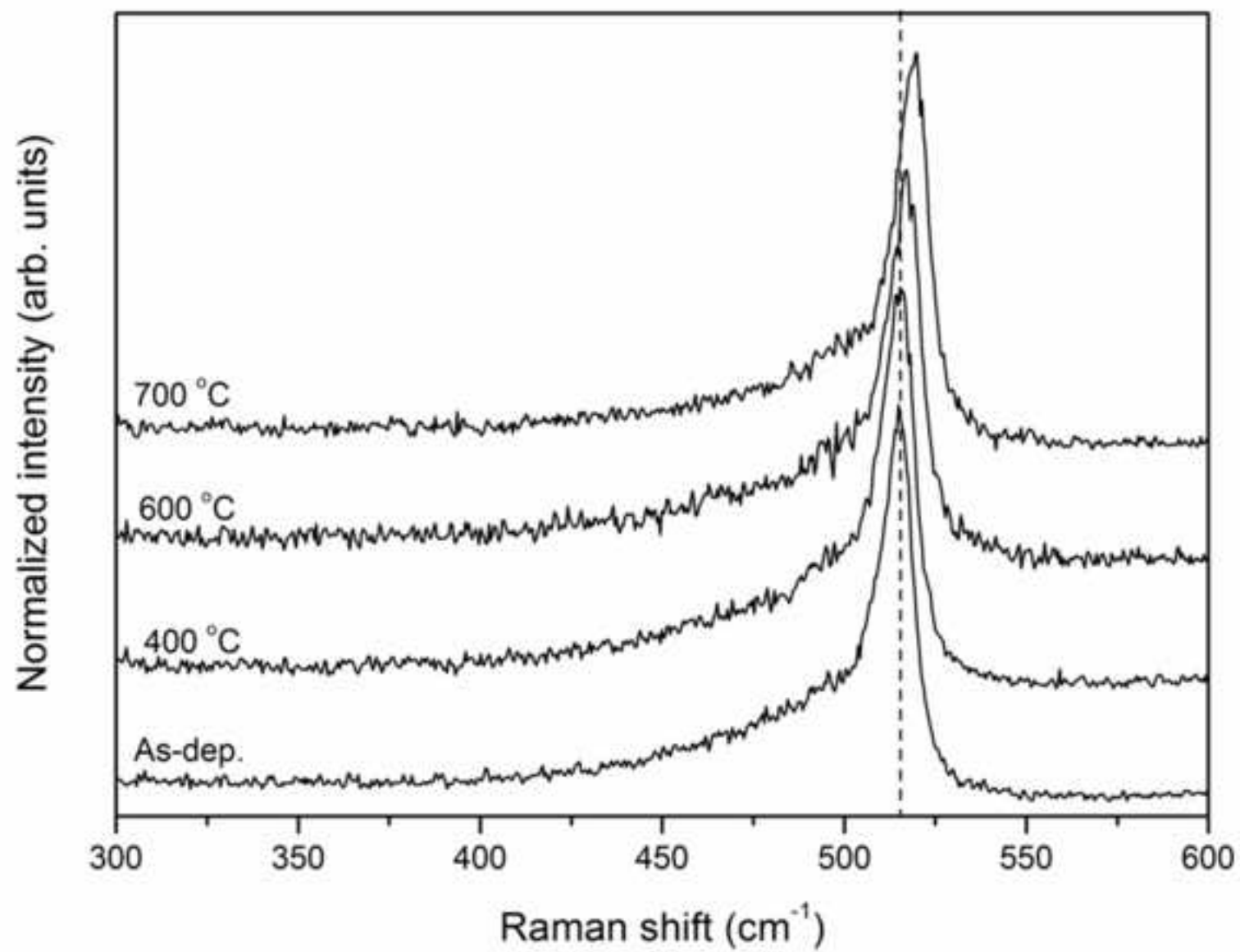


Figure 4
[Click here to download high resolution image](#)

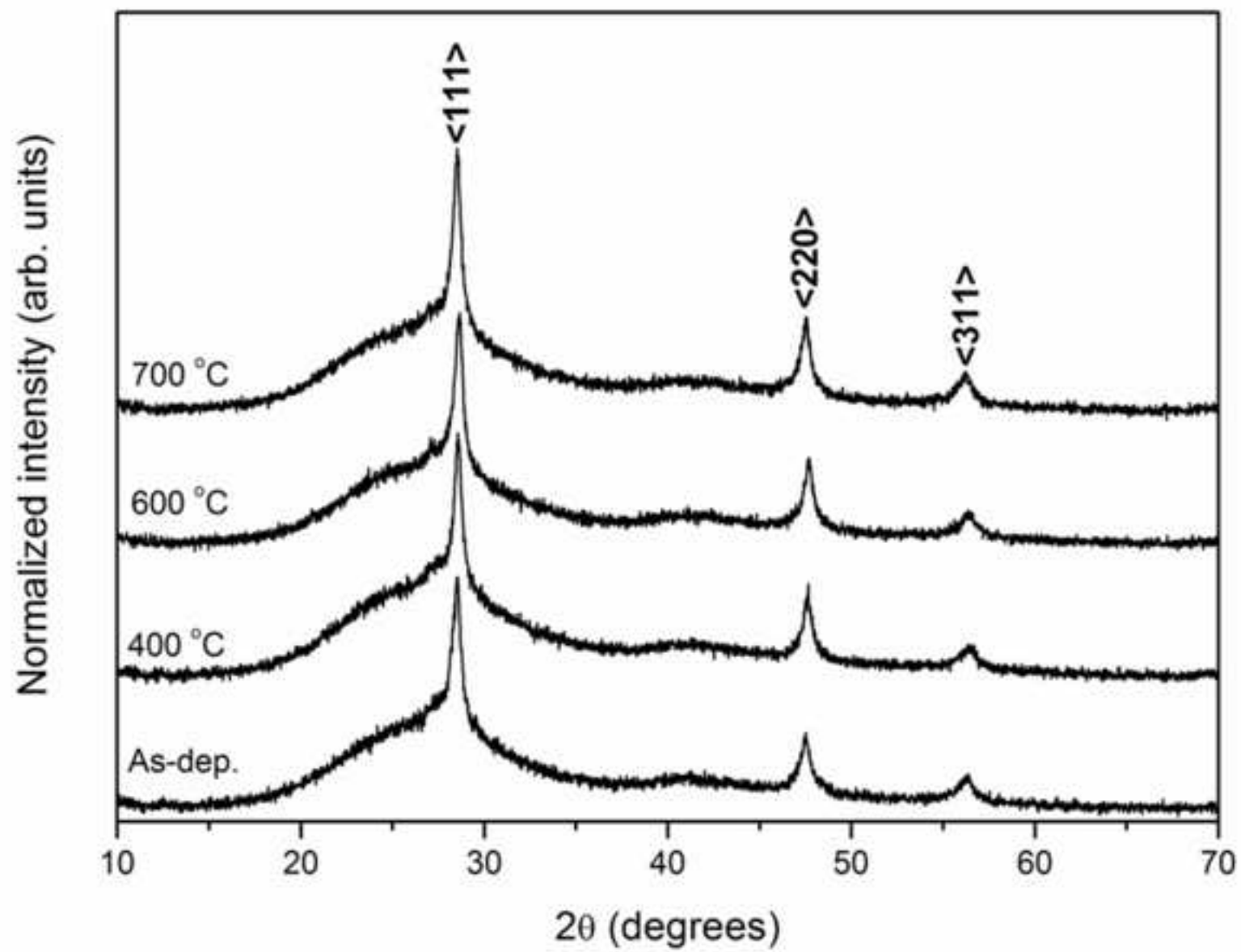


Figure 5
[Click here to download high resolution image](#)

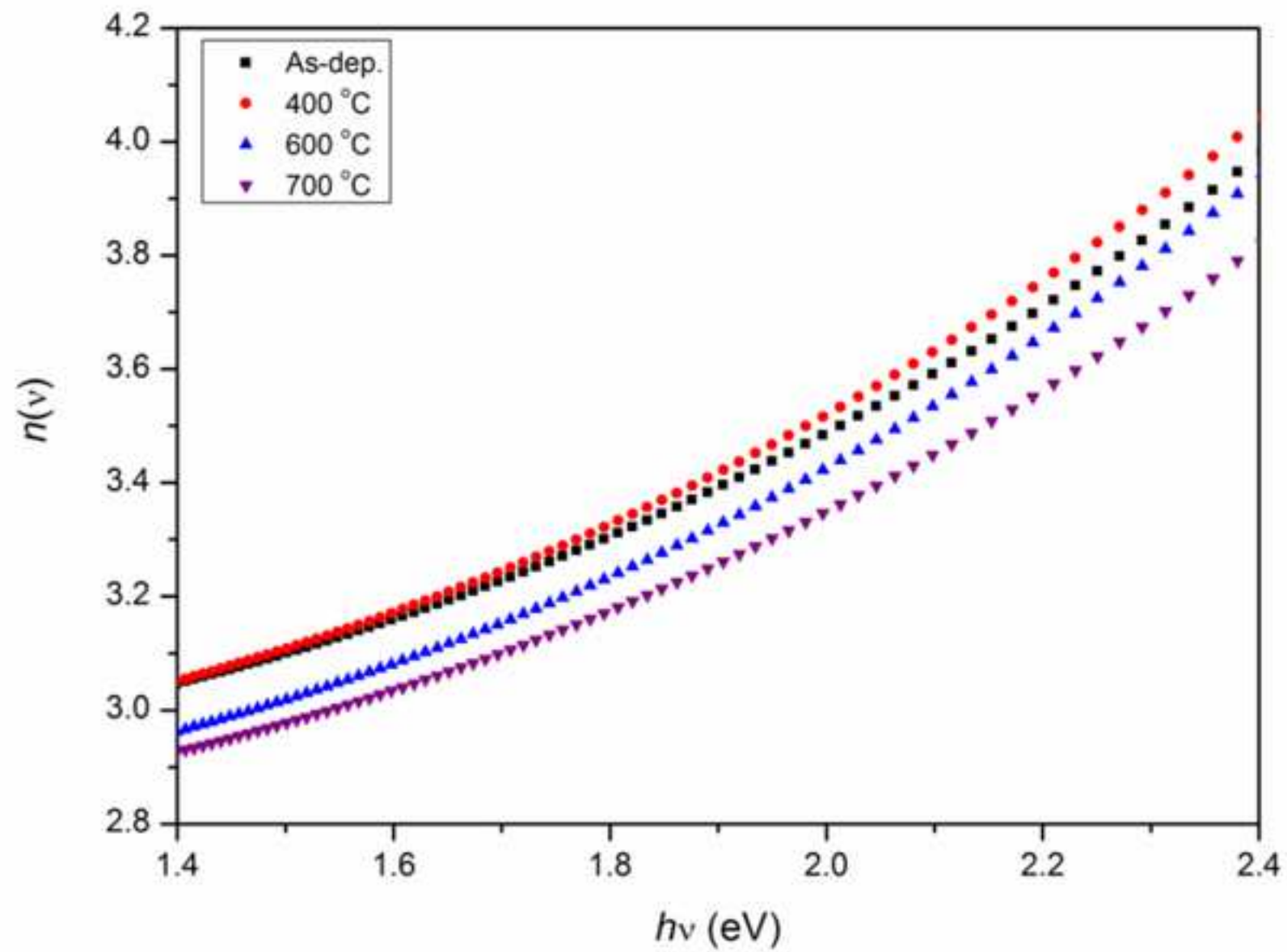


Figure 6
[Click here to download high resolution image](#)

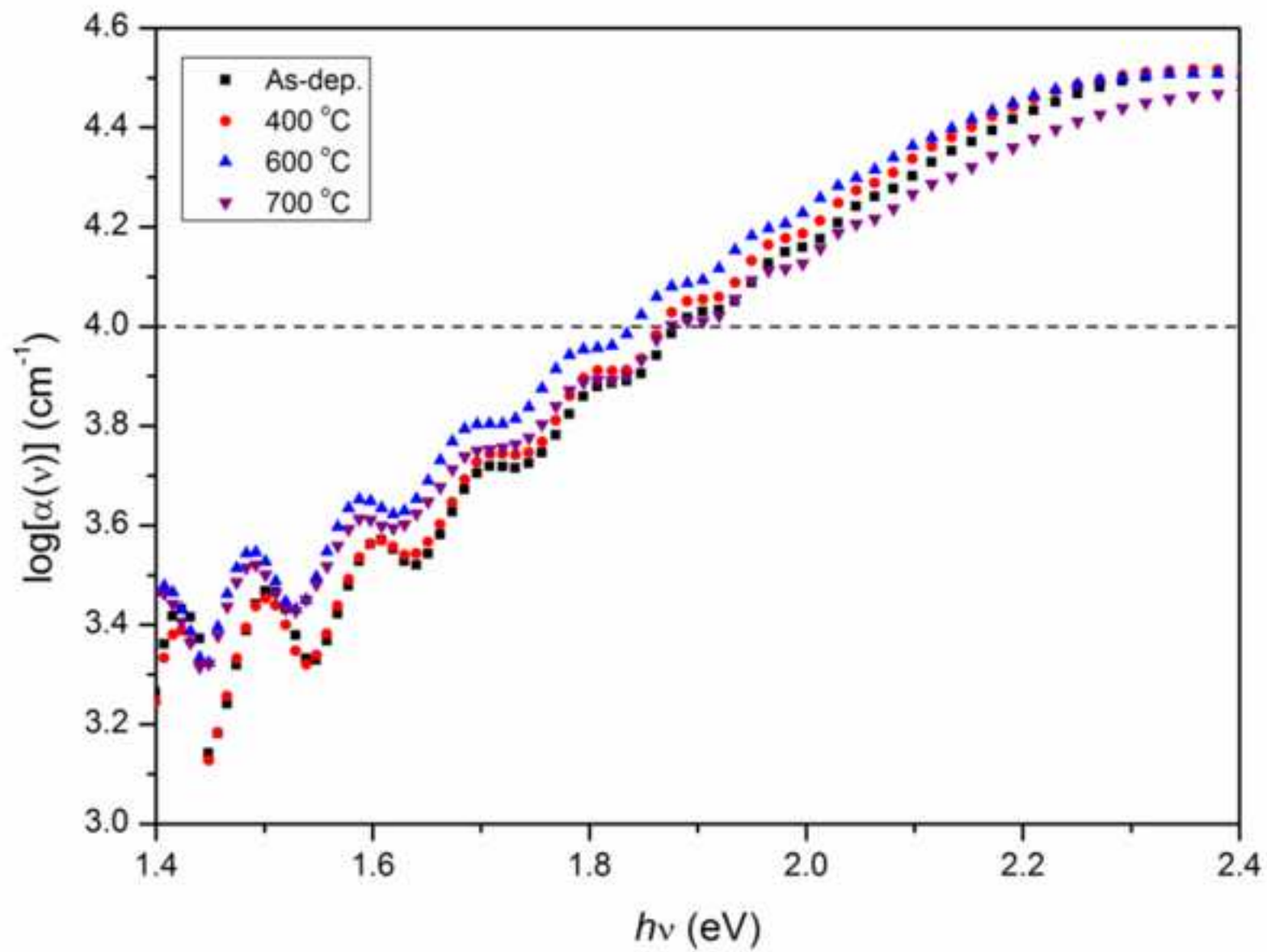


Table 1[Click here to download Table: Table 1.doc](#)

T_A (°C)	d_{Raman} (nm)	f_c (%)	n_o	E_M (eV)	E_{04} (eV)
As-dep.	3.9	53	2.750	3.11	1.88
400	4.7	57	2.758	3.05	1.87
600	5.2	59	2.668	3.03	1.84
700	8.4	64	2.651	3.10	1.87

List of Table and Figure Captions

- Table 1 Crystallite size, crystalline volume fraction and optical properties after specific annealing temperatures
- Fig. 1 FTIR absorption spectrum of the as-deposited sample and the deconvolution of the stretching vibrations (insert)
- Fig. 2 (a) Hydrogen concentration and (b) the structure factor as a function of annealing temperature
- Fig. 3 Raman spectra of the sample in the as-deposited state and after annealing at specific temperatures
- Fig. 4 XRD spectra of the sample in the as-deposited state and after annealing at specific temperatures
- Fig. 5 Refractive index spectra of the sample in the as-deposited state and after annealing at specific temperatures
- Fig. 6 Absorption coefficient spectra of the sample in the as-deposited state and after annealing at specific temperatures